


OPEN

Conversion of methane to benzene in CVI by density functional theory study

Kun Li , Hejun Li*, Ningning Yan, Tiyuan Wang, Wei Li & Qiang Song

A density functional theory (DFT) study was employed to explore the mechanism of the conversion of methane to benzene in chemical vapor infiltration (CVI) based on the concluded reaction pathways from C₁-species to C₆-species. The geometry optimization and vibrational frequency analysis of all the chemical species and transition states (TS) were performed with B3LYP along with a basis set of 6–311 + G(d, p), and Gaussian 09 software was used to perform the study. The rate constants were calculated by KiSThelp according to the conventional transition state theory (TST), and the Wigner method was applied to acquire the tunneling correction factors. Then the rate constants were fitted to the modified Arrhenius expression in the temperature range of 800–2000 K. As for the barrierless reactions calculated in this paper, the rate constants were selected from the relating references. Through the energetic and kinetic calculations, the most favorable reaction pathway for benzene formation from methane was determined, which were mainly made of the unimolecular dissociation. The conversion trend from C₁-species to C₄-species is mainly guided by a strong tendency to dehydrogenation and the pathways from C₄-species to C₆-species are all presumed to be able to produce C₆H₆ molecule.

Chemical vapor infiltration (CVI) is a widely used method for the production of carbon/carbon (C/C) composites, which are mainly employed in the manufacture of solid rocket motor nozzles, brake discs of military and commercial aircraft, and spacecraft heat shields because of their excellent thermal and mechanical properties, like high specific modulus, high specific strength, and wear resistance at high temperature¹. It is one of the most important ways to prepare high performance C/C composites using methane as precursor^{2–10}, and the pyrolysis in the gas phase has been reported to play a significant role in the formation of C/C composites^{8,11}. To fully explain the process of the gas-phase reactions and therefore help to understand and optimize the production process of C/C composites, it is essential to study the mechanism of the homogeneous reactions involved in the gas phase.

There are some researches that have been performed to explore the mechanism of the decomposition of methane. Becker and Huttinger¹² proposed a detailed reaction scheme for pyrocarbon deposition from methane, which illustrated the reaction pathways from methane to C₆-species and was used to simulate the pyrocarbon deposition kinetics. Huttinger¹³ presented a simplified reaction scheme for the deposition process from methane which helped to explain the deposition chemistry and kinetics. Kahle *et al.*¹⁴ studied the reaction pathways of the conversion of methane and concluded that coke precursor was produced from methane. Hiblot *et al.*¹⁵ performed an experimental and modeling study for the pyrolysis of methane and found that the methyl radical formed from methane mainly combined with another methyl radical to form C₂-species and the H₂ molecule could strongly limit the formation of C₂-species. Although the above researches studied the decomposition of methane, they were unable to illustrate the nature of the mechanism of the homogeneous reactions during the pyrolysis of methane, and these results could not be explained from the view of the molecular level. Besides, the presence of the species formed during the decomposition process could not easily be detected and distinguished using the online analysis instruments, which made it quite difficult to explore the corresponding mechanisms.

Nowadays, density functional theory (DFT) has become a powerful method to study the mechanisms of the chemical reactions for its convenience and accuracy, and it has also been applied to the research of the decomposition of methane. ViCes *et al.*¹⁶ calculated the complete dehydrogenation of methane on platinum catalysis by DFT method and found that species like CH₃ and CH₂ were stabilized at edges and corners of the particles, which helped to study the surface reactivity of extended transition-metal terraces and nanoparticles. To further elucidate the reaction mechanism of the conversion of methane on the single iron sites embedded in a silica matrix, Guo *et al.*¹⁷

State Key Laboratory of Solidification Processing, Carbon/Carbon Composites Research Center, Northwestern Polytechnical University, Xi'an, 710072, China. *email: lihejun@nwpu.edu.cn

simulated the reaction profile of CH₃ radicals with DFT and displayed a simplified reaction pathway from CH₃ to C₆H₆. Huang *et al.*¹⁸ presented a DFT study on the sequential process of methane decomposition on iron oxides, which could provide a detailed explanation of the reaction mechanism at the atomistic for the design of more efficient oxygen carriers. Besides, in order to understand the activity of heterogeneous catalysis affected by nanostructure, Kozlov *et al.*¹⁹ calculated the complete methane dehydrogenation on nanostructured palladium by DFT. Despite the plenty of theoretical studies of the decomposition of methane published already, there are few DFT researches concerning the detailed conversion pathways of methane to benzene in CVI, and it is of great necessity to figure out the mechanism from the molecular level.

During the decomposition of methane in CVI, benzene is a basic element of pyrolytic aromatic hydrocarbons which can further form the pyrocarbon, thus the present work is performed by limiting the reaction route only to the first cyclic ring formation. In this work, a DFT study was employed to explore the mechanism of the conversion of methane to benzene in CVI based on the concluded reaction pathways from C₁-species to C₆-species. The energy profiles of each reaction were calculated and the corresponding rate constants were obtained subsequently, then the most favorable reaction pathway was proposed.

Computational Details

All the chemical species involved in the study were optimized with different spin multiplicities followed by vibrational frequency calculations to obtain the stable molecular structures that provided the lowest energy and correct geometry. In order to verify the structure of the transition states (TS) of all the chemical reactions, the frequency analysis was conducted after the geometry optimization, which turned out that each stable TS was equipped with only one imaginary frequency. Besides, the intrinsic reaction coordinate (IRC)²⁰ was performed to prove that each TS was connected to the desired reactant and product. To get the IRC results with high quality and complete curve, the max points of each IRC calculation were set to be 150 coupled with the default step size of 10. The relative energies of the species and TS were applied to figure out the corresponding reaction energies and activation energies which were used for the energy profiles. All the quantum calculations were performed with Becke three-parameter exchange and Lee, Yang and Parr correlation function (B3LYP)^{21,22} along with a basis set of 6-311 + G(d, p), and Gaussian 09²³ software was used to study all the DFT calculations.

The rate constants as a function of temperature for the reactions involved in the study were calculated by using the kinetic and statistical thermodynamical package (KiSThelP)²⁴ according to the conventional transition state theory (TST)²⁵. The parameters required by TST such as molecular energy, spin multiplicity, and vibrational frequencies were obtained from the Gaussian output files. As for the quantum tunneling effect, the Wigner method^{26,27} was applied to acquire the tunneling correction factors for all the elementary reactions. Besides, the total reaction degeneracies of each case were taken into account by multiplying a symmetry number of each reaction by the number of equivalent abstractable hydrogen atoms²⁸. Finally, the rate constants were fitted to the modified Arrhenius expression^{26,28} in the temperature range of 800–2000 K. The formula is expressed as:

$$k(T) = A \times T^n \times \exp\left(\frac{-E_a}{RT}\right) \quad (1)$$

where A is the Arrhenius prefactor, T is the temperature, E_a is the barrier height, and n is the temperature exponent indicating the deviation from the standard Arrhenius equation. In addition, due to the fact that KiSThelP is only programmed for the reactions with TS, and for the barrierless reactions calculated in this paper, the rate constants were selected from the relative references published before.

Results and Discussion

The primary goal of this section is to obtain the main reaction pathways of the decomposition of methane during CVI by distinguishing the pathways collected from the previous researches^{11,12,29–40}. By studying and summarizing the related researches published previously, detailed reaction schemes for benzene to be prepared using methane as precursor are summarized, as shown in Fig. 1. Since there are some species produced during the decomposition of methane that make little impact on the mechanism of the formation of pyrolytic carbon, it is generally accepted that only the important molecules and radicals which determine the mechanism of the pyrolysis are supposed to be focused on. As a matter of fact, it is widely agreed that the decomposition and formation of hydrocarbon are fundamentally a free-radical mechanism¹¹, so most of the concluded reactions are radical ones. As depicted in Fig. 1, from inside to outside, it shows the conversion pathway from methane to C₂-species, C₄-species and C₆-species, respectively.

The molecular structures of all the reactants and products studied in this work are displayed in Fig. 2 ranging from hydrogen molecule to benzene. As can be seen from this figure, apart from the common species with only one specific structure, there are some isomers in this paper such as C₆H₆ that has four different chemical structures. The reaction pathways proposed in the following are all involved with the dominant species mentioned above.

Reaction pathways from C₁-species to C₂-species. For the discussion on the mechanism of reaction pathways from C₁-species to C₂-species, the reaction profiles containing every reaction pathway and their potential energies are displayed in Fig. 3, where the energies of each species and TS have been plotted relative to the total energy of the reactants that are all set to be 0 kJ/mol^{41,42}. The reactions contributing to the same product have been divided into the same column, which are arranged from left to right in substantially the order of the formation of hydrocarbon shown in Fig. 1.

The initial step of the whole reaction system is the dehydrogenation of CH₄ molecule, which decomposes directly into CH₃ radical and H atom with the endoergic energy of 463.7 kJ/mol, and this is consistent with the

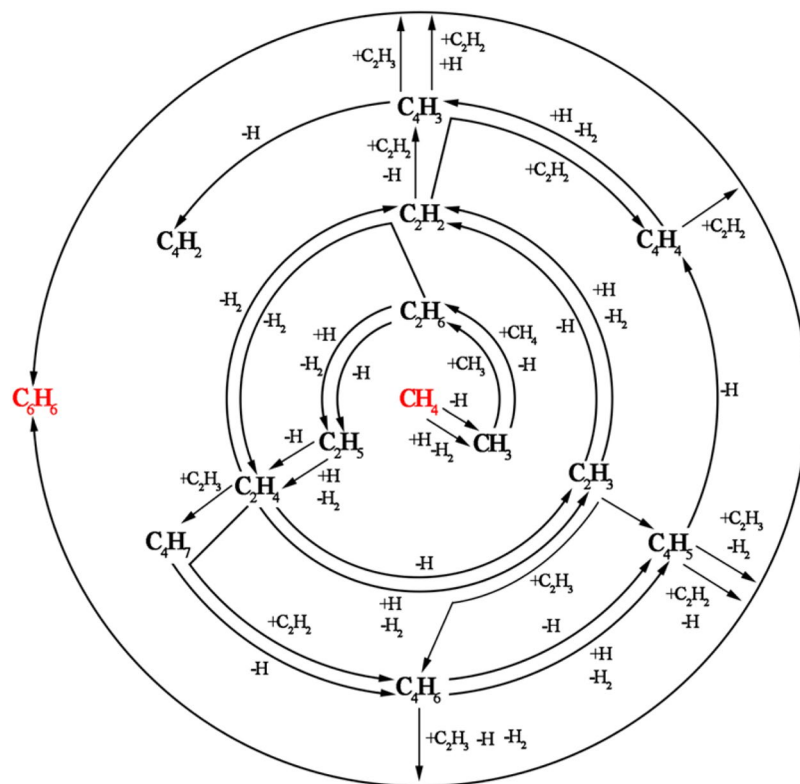


Figure 1. Detailed reaction scheme about the conversion way of methane to benzene.

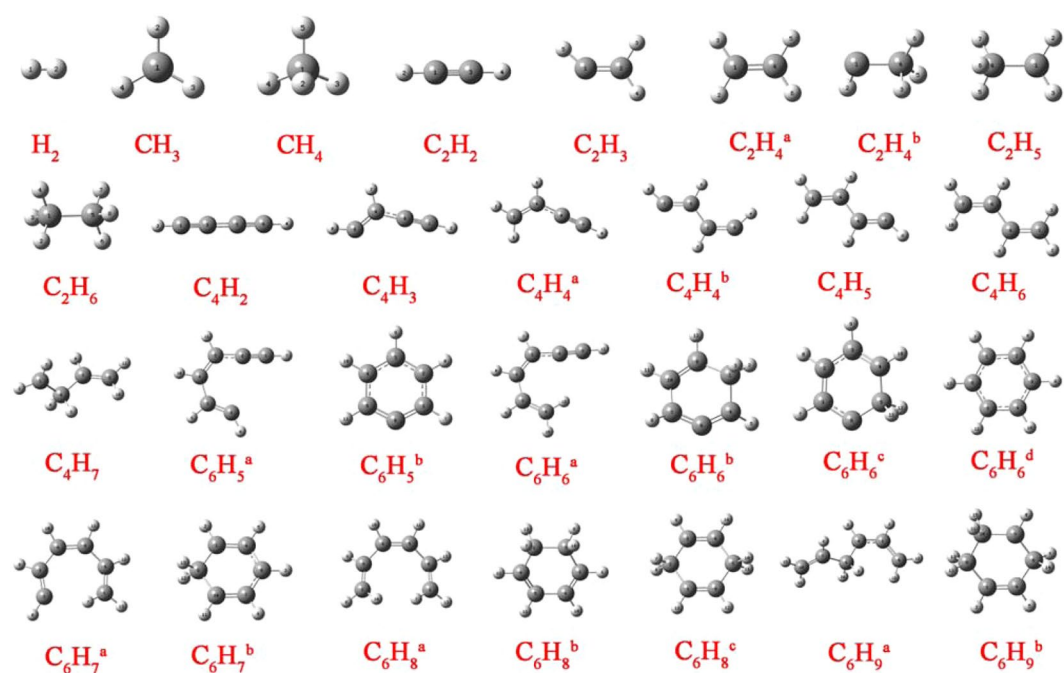


Figure 2. Optimized geometries of various reactants and products involved in the conversion of methane to benzene.

results calculated before^{17,43,44}, which proves the accuracy of this calculation method. With H atom generated, it can combine with CH_4 molecule to produce CH_3 radical and H_2 molecule through TS1 with the activation energy of 40.1 kJ/mol. At the second column, two methyl can bond together to produce an ethane molecule, which is a barrierless process with the exothermic energy of 383.9 kJ/mol. The methyl can also react with methane to yield

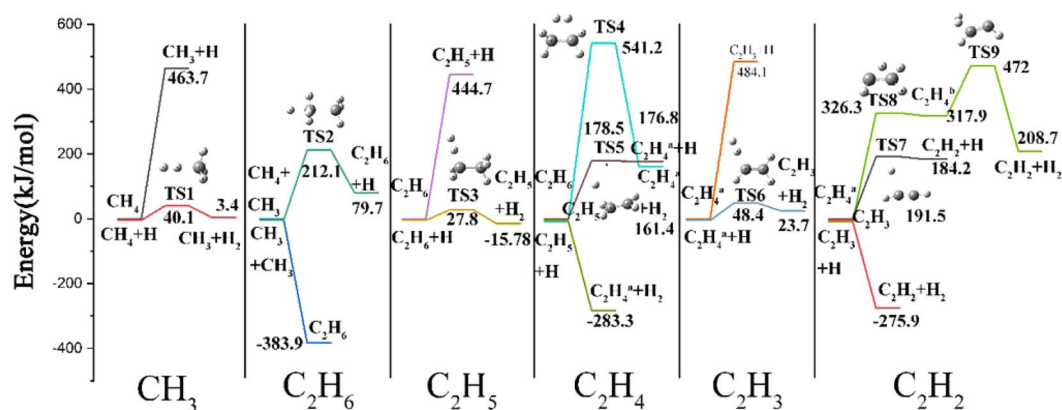


Figure 3. The pathways and the potential energy of the reactions from C₁-species to C₂-species.

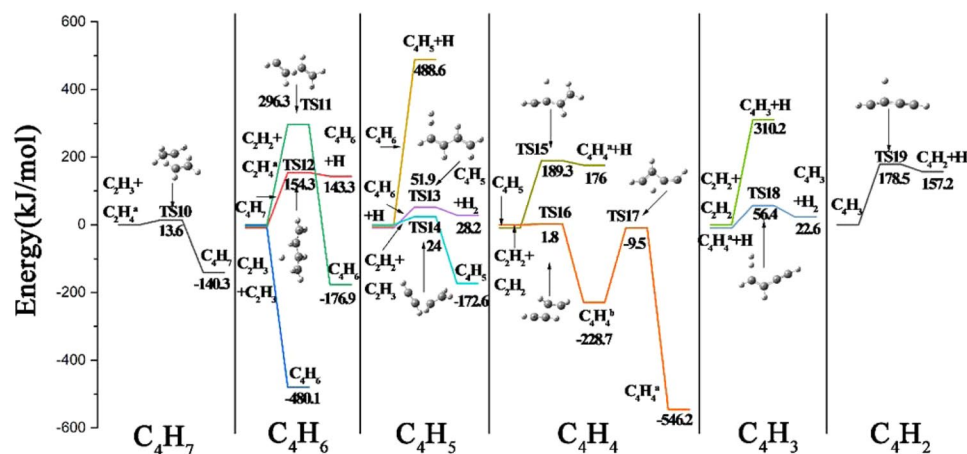


Figure 4. The pathways and the potential energy of the reactions from C₂-species to C₄-species.

ethane and hydrogen atom by overcoming the energy barrier of 212.1 kJ/mol, and the total energy of the products is 79.7 kJ/mol higher than that of the reactants. At the column of C₂H₅, C₂H₆ molecule can be abstracted by an external H atom to form C₂H₅ radical and H₂ molecule by conquering the energy barrier of 27.8 kJ/mol corresponding to TS3, and the energy of products lies 15.8 kJ/mol below the reactants. C₂H₆ molecule can also undergo H-elimination reaction forming C₂H₅ radical and H atom with the barrierless endothermic energy of 444.7 kJ/mol. As for the formation of C₂H₄ molecule, it can come from both C₂H₆ molecule and C₂H₅ radical. After overcoming the high energy barrier of 541.2 kJ/mol, C₂H₄ molecule and H₂ molecule can be produced from C₂H₆ molecule with the reaction energy being 161.4 kJ/mol, indicating an endothermic reaction. C₂H₅ radical can decompose into C₂H₄ molecule and H atom by the dehydrogenation reaction, of which the activation energy and reaction energy are 178.5 kJ/mol and 176.8 kJ/mol, respectively. This column also involves the abstraction of H atom from C₂H₅ radical by an external H atom to form C₂H₄ molecule and H₂ molecule with the barrierless reaction energy lying 283.3 kJ/mol below the reactants. The fifth column shows two endothermic reactions to the formation of C₂H₃ radical. By losing one H atom of C₂H₄ molecule, C₂H₃ radical can be produced with the high barrierless reaction energy being 484.1 kJ/mol. And with an extraneous H atom attacking C₂H₄ molecule, the corresponding products are C₂H₃ radical and H₂ molecule with the energy barrier and reaction energy being 48.4 kJ/mol and 23.7 kJ/mol, respectively. Finally, the rightmost column of Fig. 3 shows the energy process of the formation of C₂H₂ molecule. The most complicated pathway is the formation of C₂H₂ molecule and H₂ molecule from the dehydrogenation of C₂H₄ molecule, which gets the reaction energy of 208.7 kJ/mol after overcoming the energy barriers of 326.3 kJ/mol and 472 kJ/mol corresponding to TS8 and TS9, respectively. Another endothermic reaction is the H atom elimination of C₂H₃ radical, which overcomes the energy barrier of 191.5 kJ/mol and results in the energy of products being 184.2 kJ/mol. The last reaction is exothermic and barrierless, C₂H₃ + H → C₂H₂ + H₂, and the energy of products is 275.9 kJ/mol below than that of reactants.

Reaction pathways from C₂-species to C₄-species. The aim of this section is to deal with the different reaction pathways from C₂-species to C₄-species, and the corresponding potential energies of the possible and reasonable pathways are shown in Fig. 4. As is discussed in section 3.1, the same means of expression is applied to Fig. 4, which displays the formation from C₄H₇ radical to C₄H₂ molecule.

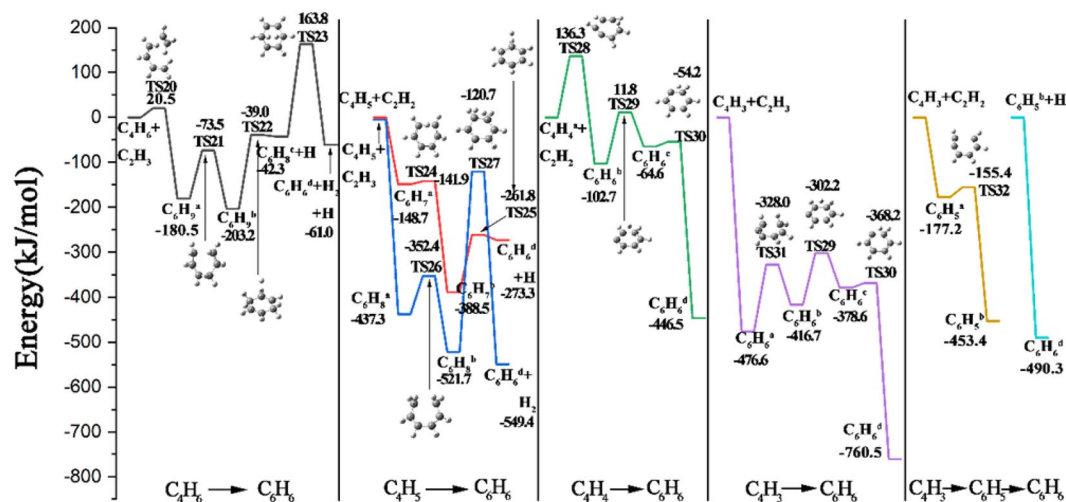


Figure 5. The pathways and the potential energy of the reactions from C_4 -species to C_6 -species.

As is depicted at the first column of Fig. 4, there is only one feasible pathway leading to C_4H_7 radical, which comes from the combination of C_2H_3 radical and C_2H_4 molecule, and the reaction energy of this exothermic process is 140.3 kJ/mol with the energy barrier of 13.6 kJ/mol. At the second column of C_4H_6 molecule, three distinct reactions are calculated. The bonding of C_2H_2 molecule and C_2H_4 molecule results to the formation of C_4H_6 molecule with releasing 176.9 kJ/mol, after undergoing TS11 with the energy barrier of 296.3 kJ/mol. C_4H_6 molecule can also be formed by the dehydrogenation of C_4H_7 radical, which requires the activation energy of 154.3 kJ/mol, and the energy of products is 143.3 kJ/mol higher than that of reactant. Another reaction leading to the appearance of C_4H_6 molecule is the radical association of two C_2H_3 radical, which is observed to be a barrierless process with the exothermic energy being 480.1 kJ/mol. With C_4H_6 molecule brought into being, the C_4H_5 radical can be generated consequently. As displayed at the third column of Fig. 4, on the one hand, by breaking one C-H bond of C_4H_6 molecule, the C_4H_5 radical is raised with the energy of the products being 488.6 kJ/mol. On the other hand, by attacking C_4H_6 molecule with an external H atom, the C_4H_5 radical can be formed as well with another product of H_2 molecule. This step is slightly endoergic (28.2 kJ/mol) and presents the energy barrier of 51.9 kJ/mol corresponding to TS13. Besides, C_4H_5 radical can also be brought out by the chemical integration of C_2H_3 radical and C_2H_2 radical, which loses 172.6 kJ/mol after conquering the energy barrier of 24 kJ/mol corresponding to TS14. At the fourth column demonstrated in Fig. 4, the formation of C_4H_4 molecule is analyzed by two reactions. Like the H-abstraction of C_4H_7 radical, C_4H_5 radical can decompose into C_4H_4 molecule and H atom by dehydrogenation, which is calculated to be endoergic (176 kJ/mol) and needs to overcome the energy barrier of 189.3 kJ/mol. Another reaction is the combination of two acetylene molecules, which goes through one intermediate of $C_4H_4^b$ radical and two transition states of TS16 and TS17. This complicated process needs to overcome a small energy barrier of TS16 to form $C_4H_4^b$, the energy of which is 228.7 kJ/mol lower than that of the reactants, and then $C_4H_4^b$ radical is transformed into the more stable structure of $C_4H_4^a$ molecule after overcoming the barrier energy of TS17. As can be observed from the structures of $C_4H_4^a$ molecule, $C_4H_4^b$ radical and TS17, which are illustrated in Figs. 2 and 4, $C_4H_4^a$ molecule is transformed from $C_4H_4^b$ radical by moving one H atom to the end of the carbon chain. At the fifth column of Fig. 4, the interaction of two acetylene molecules contributes to the presence of C_4H_3 radical and H atom, which is calculated to be barrierless and endothermic. Another endothermic reaction is the interaction of $C_4H_4^a$ molecule and H forming C_4H_3 radical and H_2 molecule with the energy of 22.6 kJ/mol, which undergoes TS18 of 56.4 kJ/mol. The last part of this diagram is the formation of C_4H_2 molecule, which is produced by abstracting the H atom of C_4H_3 radical, as can be seen from the structure of TS19. The energies of TS19 and the products are 178.5 kJ/mol and 157.2 kJ/mol, respectively.

Reaction pathways from C_4 -species to C_6 -species. This part discusses the reaction pathways leading to benzene, which is originated from C_4H_6 molecule, C_4H_5 radical, C_4H_4 molecule, and C_4H_3 radical, respectively. All the reactions analyzed in the following are multistep which are more complicated than the reactions from C_1 -species to C_4 -species, and they are divided into five columns for the convenience of discussion, as shown in Fig. 5. Unlike the other two figures discussed above, due to the fact that all these series of reactions result in the same product, benzene, Fig. 5 puts the reactions with the same main reactants into one column, such as the second column of $C_4H_5 \rightarrow C_6H_6$.

As depicted in the left column of Fig. 5, there is just one reasonable pathway resulting in benzene from C_4H_6 molecule, and four transition structures can be found. This process is initiated by the chemical combination of C_4H_6 molecule and C_2H_3 radical that brings $C_6H_9^a$ radical into existence after overcoming the small energy barrier of 20.5 kJ/mol. Then $C_6H_9^a$ radical undergoes a ring closure reaction after overcoming the activation energy of TS21 to form $C_6H_9^b$ molecule, which lies 203.2 kJ/mol below the reactants. And for the reaction to proceed further, benzene can arise from the dehydrogenation of $C_6H_9^b$ molecule followed by subsequent decomposition of $C_6H_8^c$ molecule into C_6H_6 molecule and H_2 molecule, which goes through two TS configurations of TS22 and TS23. At the second column, the interactions between C_4H_5 radical and C_2H_2 molecule or C_2H_3 radical are

calculated separately. The addition of C_2H_2 molecule takes place on C_4H_5 radical to form $C_6H_7^a$ radical, which turns out to be a barrierless and exothermic process with the energy below than that of the reactants by 148.7 kJ/mol. Then $C_6H_7^a$ radical undergoes a ring closure step after overcoming a small energy barrier of TS24 to produce a more stable structure of $C_6H_7^b$ radical, which lies 388.5 kJ/mol below the group of C_4H_5 radical and C_2H_2 molecule. After that, the C-H bond scission happens to $C_6H_7^b$ radical to generate benzene molecule and H atom, and TS25 is observed during this endothermic step with the energy of the final products being 273.3 kJ/mol lower when compared to the initial reactants. As for the addition of C_2H_3 radical to C_4H_5 radical, the whole process is very similar to the addition from C_2H_2 radical to C_4H_5 radical. At first, $C_6H_8^a$ molecule is produced with its energy lower than the reactants by 437.3 kJ/mol after the chemical integration of C_2H_3 radical and C_4H_5 radical, which is proved to be barrierless and exothermic. And $C_6H_8^a$ molecule is then transformed into $C_6H_8^b$ molecule by the ring closure step, which needs to conquer the energy barrier of TS26 and release energy to achieve the stable structure of $C_6H_8^b$ molecule with its energy lying 521.7 kJ/mol below the reactants. Further, in the third step of this route, two neighboring hydrogen atoms of $C_6H_8^b$ molecule ruptured from C-H bonds tend to form a dihydrogen molecule leaving a stable benzene molecule, which needs to overcome the high activation energy of TS27.

As displayed in the middle column of Fig. 5, the coupling of C_4H_4 molecule and C_2H_2 molecule resulting in benzene is calculated, which undergoes three transition structures TS28, TS29 and TS30, respectively. The first step of this route is exothermic (-102.7 kJ/mol) and presents the activation energy of 136.3 kJ/mol, which brings the $C_6H_6^b$ species out. Then there are two steps of H atom migration on $C_6H_6^b$ species leading to benzene molecule eventually after overcoming the energy barriers of TS29 and TS30, respectively. And the energy of the benzene molecule is 446.5 kJ/mol lower than that of the beginning reactants showing the exothermicity of this process. As for the fourth column of Fig. 5, at first glance, the chemical mechanism for this route seems as complicated as that described for the conversion from C_4H_4 molecule to benzene molecule. It begins with the addition of C_2H_3 radical to C_4H_3 radical forming $C_6H_6^a$ species by releasing 476.6 kJ/mol without overcoming the energy barrier. Then $C_6H_6^a$ species is converted to $C_6H_6^b$ species by conquering the activation energy of TS31. From the next step on, the following process is exactly the same as the conversion from $C_6H_6^b$ species to benzene molecule described in the third column except for the absolute values marked in Fig. 5. Finally, in the last column of Fig. 5, it demonstrates the conversion from C_4H_3 radical to the benzene molecule. Actually, this process is composed of two separate reactions, which is connected by the $C_6H_5^b$ radical. At first, the chemical bonding of species C_4H_3 radical and C_2H_2 molecule takes place resulting in the presence of $C_6H_5^a$ radical, which releases 177.2 kJ/mol without any activation energy. Then $C_6H_5^a$ radical is converted to a phenyl radical after overcoming the slight energy barrier of TS32. Due to the instability of phenyl radical, it is very possible for it to bond with an external H atom to form benzene molecule, which is calculated to be barrierless and releases the energy of 490.3 kJ/mol. Because the external H atom is added during this process rather than in the beginning, it makes sense to draw the energy profiles of these two reactions separately to illustrate this process more clearly and correctly.

Reaction kinetics. To figure out the reactions among those discussed above that play important roles during the conversion of methane to benzene, reaction kinetics of the elementary reactions were calculated and used for kinetic simulations, as illustrated below.

Table 1 provides the kinetic parameters for elementary reactions with TS among the reactions of C_1 – C_6 in the temperature range of 800–2000 K which covers the possible formation temperature of the species studied in this work, and for the benefit of the analysis of the mechanisms of these reactions the rate constants of the corresponding reactions in the temperature of 1353 K are listed individually because this temperature is very special during the decomposition of methane by using CVI method⁹. As is shown in Table 1, the kinetic parameters for the 32 reactions differ greatly with each other with the difference of the class and progress of the reactions. For example, the lowest reaction rate in 1353 K is $4.30 \times 10^{-22} \text{ cm}^3 \text{ mol}^{-1} \text{ s}^{-1}$ of $C_2H_2 + C_2H_4 \rightarrow C_4H_6$, and the highest reaction rate in 1353 K is $1.52 \times 10^{12} \text{ cm}^3 \text{ mol}^{-1} \text{ s}^{-1}$ of $C_6H_6^c \rightarrow C_6H_6^d$, which shows a difference of 34 orders of magnitude between these two reaction rates.

Table 2 displays the reaction rates for 13 elementary reactions without TS among the reactions of C_1 – C_6 . Because the KiSThelP is unable to calculate the rate constants of the barrierless reactions, the corresponding rate values are taken from the literatures by searching the NIST chemical kinetics database⁴⁵. To the best of our knowledge, there are no relevant theoretical or experimental results about the rate constants for the reaction $C_4H_3 + C_2H_3 \rightarrow C_6H_6^a$, and as a result, this specific reaction is disappeared in Table 2. As can be seen, almost all the rate constants are selected at the temperature of 1400 K which is close to 1353 K and can be valuable as well, except for the reaction $C_2H_3 + C_2H_3 \rightarrow C_4H_6$ whose rate constant is elected at 298 K because of the lack of its kinetic study at high temperatures. Like Table 1, the rate constants of these barrierless reactions disperse in a wide range. The smallest value is $5.00 \times 10^{-21} \text{ cm}^3 \text{ mol}^{-1} \text{ s}^{-1}$ of reaction $CH_4 \rightarrow CH_3 + H$, and the largest value is $13.70 \text{ cm}^3 \text{ mol}^{-1} \text{ s}^{-1}$ of reaction $C_2H_6 \rightarrow C_2H_5 + H$, which indicates that all the rate constants of the barrierless reactions are commonly low.

To better understand the variation tendency of the rate constants of the reactions listed in Table 1, Fig. 6 presents a comparison of those reactions, which are divided into four parts due to the different reaction classes, dehydrogenation, H-abstraction by H atom, isomerization and combination. As demonstrated in Fig. 6, through the detailed comparisons of the rate constants within the same reaction class, it is concluded that the ranges of the rate constants for dehydrogenation reactions and H-abstraction reactions are both relatively small in the temperature range of 800–2000 K when compared with the isomerization reactions and combination reactions whose rate constants vary greatly with the increase of temperature. The reason may be due to that the rate constants for similar reactions are mainly dependent on the molecular structure. In general, the rate constants of all those reactions increase with the increase of temperature, except for the reaction $C_2H_2 + C_2H_3 \rightarrow C_4H_5$ whose rate constants decrease gently with the increase of temperature, illustrated in Fig. 6d. Further, there are a few reactions showing high rate constants all the time, such as the reaction $C_6H_6^c \rightarrow C_6H_6^d$ in Fig. 6c, which is attributed to the fact that

Reaction	A	n	E _a	k (T = 1353 K)
C ₁ -C ₂				
CH ₄ + H → CH ₃ + H ₂	8.20 × 10 ⁻¹⁷	2.01	27.0	1.46 × 10 ⁻¹¹
CH ₃ + CH ₄ → C ₂ H ₆ + H	5.28 × 10 ⁻²⁴	3.52	197.3	1.38 × 10 ⁻²⁰
C ₂ H ₆ + H → C ₂ H ₅ + H ₂	1.04 × 10 ⁻¹⁶	2.04	13.7	7.45 × 10 ⁻¹¹
C ₂ H ₆ → C ₂ H ₄ + H ₂	5.08 × 10 ¹⁰	1.19	509.6	5.82 × 10 ⁻⁶
C ₂ H ₅ → C ₂ H ₄ + H	4.56 × 10 ¹¹	0.61	163.7	1.78 × 10 ⁷
C ₂ H ₄ + H → C ₂ H ₃ + H ₂	2.25 × 10 ⁻¹⁶	1.95	36.2	1.17 × 10 ⁻¹¹
C ₂ H ₃ → C ₂ H ₂ + H	1.58 × 10 ¹²	0.69	175.9	3.68 × 10 ⁷
C ₂ H ₄ ^a → C ₂ H ₄ ^b	2.41 × 10 ¹²	0.49	312.3	7.13 × 10 ¹
C ₂ H ₄ ^b → C ₂ H ₂ + H ₂	2.99 × 10 ¹¹	0.61	139.7	1.01 × 10 ⁸
C ₂ -C ₄				
C ₂ H ₃ + C ₂ H ₄ → C ₄ H ₇	1.75 × 10 ⁻²¹	3.02	14.4	1.38 × 10 ⁻¹²
C ₂ H ₂ + C ₂ H ₄ → C ₄ H ₆	3.84 × 10 ⁻²²	3.23	260.9	4.30 × 10 ⁻²²
C ₄ H ₇ → C ₄ H ₆ + H	1.23 × 10 ¹¹	0.64	138.7	5.45 × 10 ⁷
C ₄ H ₆ + H → C ₄ H ₅ + H ₂	8.23 × 10 ⁻¹⁷	1.91	41.0	2.10 × 10 ⁻¹²
C ₂ H ₂ + C ₂ H ₃ → C ₄ H ₅	2.43 × 10 ⁻¹⁹	2.52	-41.7	7.68 × 10 ⁻¹⁰
C ₄ H ₅ → C ₄ H ₄ ^a + H	9.62 × 10 ¹¹	0.67	160.6	7.61 × 10 ⁷
C ₂ H ₂ + C ₂ H ₂ → C ₄ H ₄ ^b	2.26 × 10 ⁻¹⁶	2.24	232.1	2.48 × 10 ⁻¹⁸
C ₄ H ₄ ^b → C ₄ H ₄ ^a	1.33 × 10 ¹¹	0.65	201.1	2.53 × 10 ⁵
C ₄ H ₄ ^a + H → C ₄ H ₃ + H ₂	1.08 × 10 ⁻¹⁶	1.91	45.5	1.76 × 10 ⁻¹²
C ₄ H ₃ → C ₄ H ₂ + H	7.05 × 10 ¹¹	0.71	161.5	7.04 × 10 ⁷
C ₄ -C ₆				
C ₄ H ₆ + C ₂ H ₃ → C ₆ H ₉ ^a	4.24 × 10 ⁻²²	3.01	19.7	1.94 × 10 ⁻¹³
C ₆ H ₉ ^a → C ₆ H ₉ ^b	9.20 × 10 ¹⁰	0.11	106.6	1.51 × 10 ⁷
C ₆ H ₉ ^b → C ₆ H ₈ ^c + H	7.60 × 10 ¹¹	0.64	149.3	1.30 × 10 ⁸
C ₆ H ₈ ^c → C ₆ H ₆ ^d + H ₂	1.67 × 10 ⁹	1.00	180.7	2.47 × 10 ⁵
C ₆ H ₇ ^a → C ₆ H ₇ ^b	6.70 × 10 ¹¹	0.06	5.6	6.23 × 10 ¹¹
C ₆ H ₇ ^b → C ₆ H ₆ ^d + H	4.68 × 10 ¹¹	0.60	112.5	1.55 × 10 ⁹
C ₆ H ₈ ^a → C ₆ H ₈ ^b	1.35 × 10 ¹¹	0.09	82.9	1.66 × 10 ⁸
C ₆ H ₈ ^b → C ₆ H ₆ ^d + H ₂	5.65 × 10 ⁹	1.20	379.1	7.42 × 10 ⁻²
C ₄ H ₄ ^a + C ₂ H ₂ → C ₆ H ₆ ^b	2.13 × 10 ⁻²²	2.62	67.4	8.45 × 10 ⁻¹⁷
C ₆ H ₆ ^b → C ₆ H ₆ ^c	6.11 × 10 ¹¹	0.35	105.2	6.71 × 10 ⁸
C ₆ H ₆ ^c → C ₆ H ₆ ^d	8.71 × 10 ¹¹	0.16	6.4	1.52 × 10 ¹²
C ₆ H ₆ ^a → C ₆ H ₆ ^b	6.26 × 10 ¹⁰	0.16	144.9	5.06 × 10 ⁵
C ₆ H ₅ ^a → C ₆ H ₅ ^b	1.02 × 10 ¹²	-0.02	21.0	1.37 × 10 ¹¹

Table 1. Kinetic parameters for elementary reactions with transition states among the reactions of C₁-C₆. Rate constants are fitted in the modified Arrhenius form ($k = AT^n e^{-E_a/RT}$) in the temperature range of 800–2000 K. Values of the parameters A and E_a are in units of cm³ s⁻¹ molecule⁻¹ and kJ mol⁻¹, respectively. Values of k (T) are reported at 1353 K.

the less stable radical has changed into the reasonably stabilized molecule with low energy. In addition, there are another 4 reactions that are not included in Fig. 6, C₂H₆ → C₂H₄ + H₂, C₂H₄^b → C₂H₂ + H₂, C₆H₈^b → C₆H₆^d + H₂ and C₆H₈^c → C₆H₆^d + H₂. Obviously, the dissociation of these 4 reactions is quite different from the previous four reaction classes, and the difference of the orders of magnitude among these four reaction rates are too large to be plotted in one figure. However, the rate constants of these reactions still increase with the increase of temperature.

General Discussion

It is widely accepted that all the reactions proposed above are possible pathways for the overall process of the conversion of methane to benzene in CVI. Furthermore, based on the above analysis, the most preferred pathway can be identified by comparing the potential energies and rate constants of the reactions resulting in the same products, concluded in Table 3. On the one hand, the exothermic reactions are more preferred than the endothermic reactions. For example, for the production of C₂H₆ molecule in Fig. 3, the reaction CH₃ + CH₃ → C₂H₆ has an advantage over the reaction CH₃ + CH₄ → C₂H₆ + H because of its exothermicity. On the other hand, the reactions with higher rate constants are more favorable. For instance, between the two reactions forming C₂H₅ radical in Fig. 3, the reaction C₂H₆ → C₂H₅ + H is preferential rather than the reaction C₂H₆ + H → C₂H₅ + H₂ because the rate constant of the former reaction is 11 orders of magnitude higher than that of the latter one. And by adopting the two rules into all the reactions, the concluded main pathway is drawn in Fig. 7. Meanwhile, the high energy inputs required for some of the reactions are provided by the high-temperature environment. As for the pathways from C₄-species to C₆-species, each reaction route is composed of at least three steps and exhibits

Reaction	k (T)	References
C ₁ -C ₂		
CH ₄ → CH ₃ + H	k (1400 K) = 5.00 × 10 ⁻²¹	46
CH ₃ + CH ₃ → C ₂ H ₆	k (1400 K) = 3.04 × 10 ⁻¹¹	47
C ₂ H ₆ → C ₂ H ₅ + H	k (1400 K) = 13.70	48
C ₂ H ₅ + H → C ₂ H ₄ ^a + H ₂	k (1400 K) = 3.01 × 10 ⁻¹²	49
C ₂ H ₄ ^a → C ₂ H ₃ + H	k (1400 K) = 0.13	50
C ₂ H ₃ + H → C ₂ H ₂ + H ₂	k (1400 K) = 2.01 × 10 ⁻¹¹	51
C ₂ -C ₄		
C ₂ H ₃ + C ₂ H ₃ → C ₄ H ₆	k (298 K) = 9.50 × 10 ⁻¹¹	52
C ₄ H ₆ → C ₄ H ₅ + H	k (1400 K) = 1.04	53
C ₂ H ₂ + C ₂ H ₂ → C ₄ H ₃ + H	k (1200 K) = 1.60 × 10 ⁻²⁴	54
C ₄ -C ₆		
C ₂ H ₂ + C ₄ H ₅ → C ₆ H ₇ ^a	k (1400 K) = 1.31 × 10 ⁻¹⁴	55
C ₂ H ₃ + C ₄ H ₅ → C ₆ H ₈ ^a	k (1400 K) = 1.39 × 10 ⁻¹¹	55
C ₄ H ₃ + C ₂ H ₂ → C ₆ H ₅ ^a	k (1400 K) = 3.20 × 10 ⁻¹⁴	55
C ₆ H ₅ + H → C ₆ H ₆ ^d	k (1400 K) = 2.05 × 10 ⁻¹⁰	56

Table 2. Kinetic parameters for elementary reactions without transition states among the reactions of C₁-C₆. Values of k (T) are taken from the literatures.

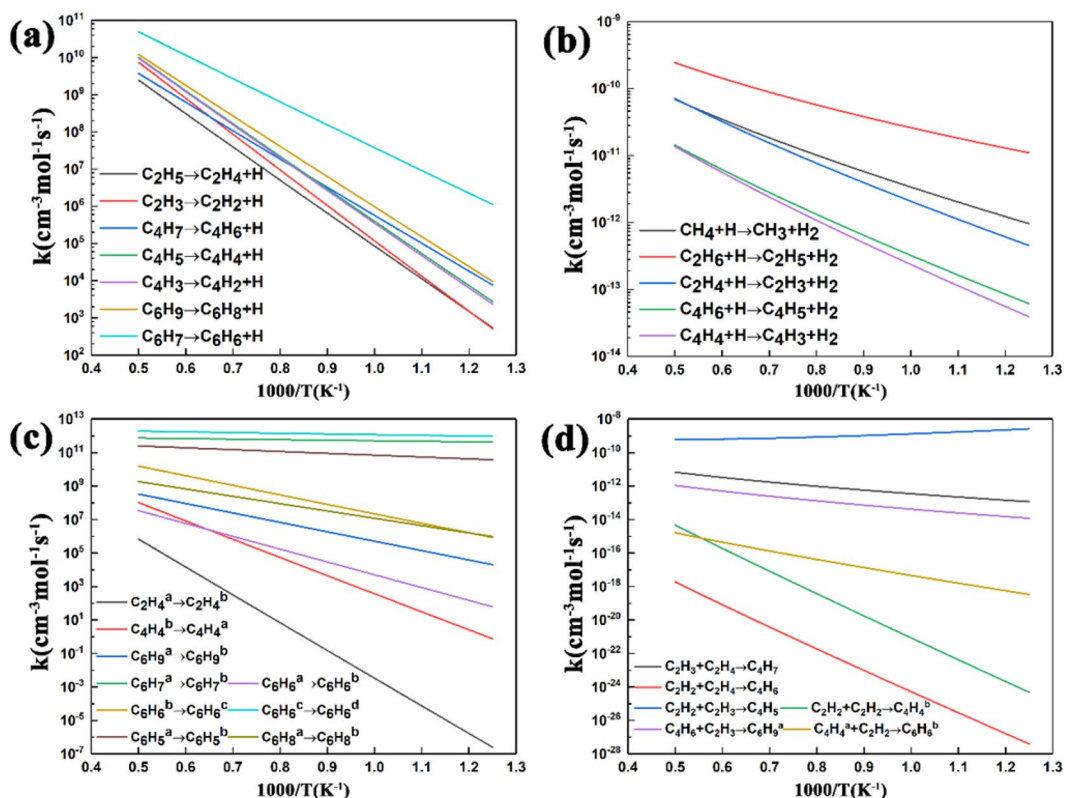


Figure 6. Comparisons of calculated rate constants for (a) dehydrogenation, (b) H-abstraction by H atom, (c) isomerization and (d) combination among the reactions of C₁-C₆.

similar potential energies and rate constants, which makes it quite difficult to distinguish the most favorable route among these reactions. Consequently, it is inferred that C₆H₆ molecule can be possibly produced through all these routes shown in Fig. 5.

As depicted in Fig. 7, the most fundamental and initial step of this route is the dehydrogenation of CH₄ molecule which is the original material of the process, even though this step takes a lot of energy to proceed and has a low rate constant. Besides, the dehydrogenation effect plays a significant role in the whole process. The C₂H₄ molecule, C₂H₃ radical, and C₂H₂ molecule produced during the dehydrogenation can help the reactions of C₄-species to perform further, and C₂H₃ radical and C₂H₂ molecule can also take part in the production of C₆H₆.

Product	Reactions	Type	k	Main reaction
CH ₃	CH ₄ + H → CH ₃ + H ₂	exothermic	1.46 × 10 ⁻¹¹	CH ₄ → CH ₃ + H
	CH ₄ → CH ₃ + H	endothermic	5.00 × 10 ⁻²¹	
C ₂ H ₆	CH ₃ + CH ₄ → C ₂ H ₆ + H	endothermic	1.38 × 10 ⁻²⁰	CH ₃ + CH ₃ → C ₂ H ₆
	CH ₃ + CH ₃ → C ₂ H ₆	exothermic	3.04 × 10 ⁻¹¹	
C ₂ H ₅	C ₂ H ₆ + H → C ₂ H ₅ + H ₂	exothermic	7.45 × 10 ⁻¹¹	C ₂ H ₆ → C ₂ H ₅ + H
	C ₂ H ₆ → C ₂ H ₅ + H	endothermic	13.70	
C ₂ H ₄	C ₂ H ₆ → C ₂ H ₄ + H ₂	endothermic	5.82 × 10 ⁻⁶	C ₂ H ₅ → C ₂ H ₄ + H
	C ₂ H ₅ → C ₂ H ₄ + H	endothermic	1.78 × 10 ⁷	
	C ₂ H ₅ + H → C ₂ H ₄ ^a + H ₂	exothermic	3.01 × 10 ⁻¹²	
C ₂ H ₃	C ₂ H ₄ + H → C ₂ H ₃ + H ₂	endothermic	1.17 × 10 ⁻¹¹	C ₂ H ₄ ^a → C ₂ H ₃ + H
	C ₂ H ₄ ^a → C ₂ H ₃ + H	endothermic	0.13	
C ₂ H ₂	C ₂ H ₃ → C ₂ H ₂ + H	endothermic	3.68 × 10 ⁷	C ₂ H ₃ → C ₂ H ₂ + H
	C ₂ H ₃ + H → C ₂ H ₂ + H ₂	exothermic	2.01 × 10 ⁻¹¹	
C ₄ H ₇	C ₂ H ₃ + C ₂ H ₄ → C ₄ H ₇	exothermic	1.38 × 10 ⁻¹²	C ₂ H ₃ + C ₂ H ₄ → C ₄ H ₇
C ₄ H ₆	C ₂ H ₂ + C ₂ H ₄ → C ₄ H ₆	exothermic	4.30 × 10 ⁻²²	C ₄ H ₇ → C ₄ H ₆ + H
	C ₄ H ₇ → C ₄ H ₆ + H	endothermic	5.45 × 10 ⁷	
	C ₂ H ₃ + C ₂ H ₃ → C ₄ H ₆	exothermic	9.50 × 10 ⁻¹¹	
C ₄ H ₅	C ₄ H ₆ + H → C ₄ H ₅ + H ₂	endothermic	2.10 × 10 ⁻¹²	C ₄ H ₆ → C ₄ H ₅ + H
	C ₂ H ₂ + C ₂ H ₃ → C ₄ H ₅	exothermic	7.68 × 10 ⁻¹⁰	
	C ₄ H ₆ → C ₄ H ₅ + H	endothermic	1.04	
C ₄ H ₄	C ₄ H ₅ → C ₄ H ₄ ^a + H	endothermic	7.61 × 10 ⁷	C ₄ H ₅ → C ₄ H ₄ ^a + H
C ₄ H ₃	C ₄ H ₄ ^a + H → C ₄ H ₃ + H ₂	endothermic	1.76 × 10 ⁻¹²	C ₄ H ₄ ^a + H → C ₄ H ₃ + H ₂
	C ₂ H ₂ + C ₂ H ₂ → C ₄ H ₃ + H	endothermic	1.60 × 10 ⁻²⁴	
C ₄ H ₂	C ₄ H ₃ → C ₄ H ₂ + H	endothermic	7.04 × 10 ⁷	C ₄ H ₃ → C ₄ H ₂ + H

Table 3. Comparisons of the potential energies and rate constants of the reactions.

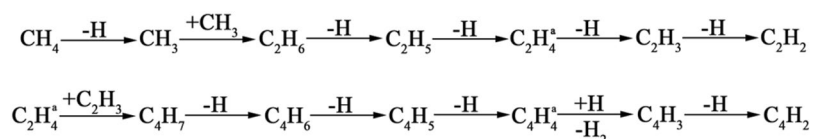


Figure 7. Main reaction route from C₁ to C₄ during the conversion of methane to benzene.

molecule. The multistep reactions forming C₆H₆ molecule are mainly attributed to the participation of C₄H₃ radical, C₄H₄ molecule, C₄H₅ radical, and C₄H₆ molecule. From Fig. 7, it can be seen that the main reaction routes are made of the unimolecular dissociation.

Conclusions

Based on the concluded pathways from methane to benzene, the DFT study was performed to explain the reaction mechanisms and corresponding kinetics, which presented the calculation results of the potential energy and Arrhenius parameters involved in the process. The reaction profiles and rate constants of each pathway from C₁-species to C₆-species were obtained and the most favorable route was proposed. The conversion trend from C₁-species to C₄-species is mainly guided by a strong tendency to dehydrogenation, which is found to play an important role in this route. And the main reaction routes are made of the unimolecular dissociation. In addition, the pathways from C₄-species to C₆-species are all presumed to be able to produce C₆H₆ molecule.

Received: 10 July 2019; Accepted: 6 December 2019;

Published online: 20 December 2019

References

- Park, S. J. Carbon/Carbon Composites. In *Carbon Fibers* (ed. Park, S. J.) 279–294 (Springer 2018).
- Li, H. *et al.* Anti-oxidation and ablation properties of carbon/carbon composites infiltrated by hafnium boride. *Carbon*. **52**, 418–26 (2013).
- Song, Q. *et al.* Carbon nanotube-multilayered graphene edge plane core-shell hybrid foams for ultrahigh-performance electromagnetic-interference shielding. *Adv Mater*. **29**(31), 1701583 (2017).
- Cheng, C. *et al.* Effects of pyrocarbon on morphology stability of SiC nanowires at high temperatures. *J Am Ceram Soc*. **101**(8), 3694–702 (2018).
- Chen, M. *et al.* High temperature oxidation resistance of La₂O₃-modified ZrB₂-SiC coating for SiC-coated carbon/carbon composites. *J Alloy Compd*. **765**, 37–45 (2018).

6. Hu, Z. J., Zhang, W. G., Hüttinger, K. J., Reznik, B. & Gerthsen, D. Influence of pressure, temperature and surface area/volume ratio on the texture of pyrolytic carbon deposited from methane. *Carbon*. **41**(4), 749–58 (2003).
7. Sun, C., Li, H., Fu, Q. & Zhang, J. Microstructure and ablation properties of carbon/carbon composites modified by ZrSiO₄. *Corros Sci*. **79**, 100–7 (2014).
8. Li, A., Norinaga, K., Zhang, W. & Deutschmann, O. Modeling and simulation of materials synthesis: Chemical vapor deposition and infiltration of pyrolytic carbon. *Compos Sci Technol*. **68**(5), 1097–104 (2008).
9. Shen, Q. *et al.* Simultaneously improving the mechanical strength and electromagnetic interference shielding of carbon/carbon composites by electrophoretic deposition of SiC nanowires. *J Mater Chem C*. **6**(22), 5888–99 (2018).
10. Song, Q. *et al.* Vertically grown edge-rich graphene nanosheets for spatial control of Li nucleation. *Adv Energy Mater*. **8**(22), 1800564 (2018).
11. Féron, O., Langlais, F. & Naslain, R. Analysis of the gas phase by *in situ* FTIR spectrometry and mass spectrometry during the CVD of pyrocarbon from propane. *Chem Vapor Depos*. **5**(1), 37–47 (1999).
12. Becker, A. & Hüttinger, K. J. Chemistry and kinetics of chemical vapor deposition of pyrocarbon — IV Pyrocarbon deposition from methane in the low temperature regime. *Carbon*. **36**, 213–224 (1998).
13. Hüttinger, K. J. CVD in hot wall reactors — The interaction between homogeneous gas-phase and heterogeneous surface reactions. *Chem Vapor Depos*. **4**(4), 151–8 (1998).
14. Kahle, L. C. S. *et al.* Methane dry reforming at high temperature and elevated pressure: Impact of gas-phase reactions. *Ind Eng Chem Res*. **52**(34), 11920–30 (2013).
15. Hiblot, H., Ziegler-Devin, I., Fournet, R. & Glaude, P. A. Steam reforming of methane in a synthesis gas from biomass gasification. *Int J Hydrogen Energ*. **41**(41), 18329–38 (2016).
16. Viñes, F. *et al.* Methane activation by platinum: Critical role of edge and corner sites of metal nanoparticles. *Chemistry - A European Journal*. **16**(22), 6530–9 (2010).
17. Guo, X. *et al.* Direct, nonoxidative conversion of methane to ethylene, aromatics, and hydrogen. *Science*. **344**, 616–619 (2014).
18. Huang, L., Tang, M., Fan, M. & Cheng, H. Density functional theory study on the reaction between hematite and methane during chemical looping process. *Appl Energ*. **159**, 132–44 (2015).
19. Kozlov, S. M. & Neyman, K. M. Insights from methane decomposition on nanostructured palladium. *J Catal*. **337**, 111–21 (2016).
20. Gonzalez, C. & Schlegel, H. B. Reaction path following in mass-weighted internal coordinates. *J. Phys. Chem*. **94**(14), 5523–5527 (1990).
21. Stephens, P. J. *et al.* *Ab initio* calculation of vibrational absorption and circular dichroism spectra using density functional force fields. *Journal of Physical Chemistry*. **98**(1–3), 247–257 (1994).
22. Becke, A. D. Density-functional thermochemistry. III. *The role of exact exchange*. *The Journal of Chemical Physics*. **98**(7), 5648–52 (1993).
23. Gaussian 09, Revision D.01, M. J. Frisch *et al.*, Gaussian, Inc., Wallingford CT, (2013).
24. Canneaux, S., Bohr, F. & Henon, E. KiSThElP: A program to predict thermodynamic properties and rate constants from quantum chemistry results. *Journal of Computational Chemistry*. **35**(1), 82–93 (2014).
25. Truhlar, D. G., Garrett, B. C. & Klippenstein, S. J. Current status of transition-state theory. *The Journal of Physical Chemistry*. **100**(31), 12771–800 (1996).
26. Georganta, E., Rahman, R. K., Raj, A. & Sinha, S. Growth of polycyclic aromatic hydrocarbons (PAHs) by methyl radicals: Pyrene formation from phenanthrene. *Combust Flame*. **185**, 129–41 (2017).
27. Raj, A. *et al.* New polycyclic aromatic hydrocarbon (PAH) surface processes to improve the model prediction of the composition of combustion-generated PAHs and soot. *Carbon*. **48**(2), 319–32 (2010).
28. Fernández-Ramos, A., Ellington, B. A., Meana-Pañeda, R., Marques, J. M. C. & Truhlar, D. G. Symmetry numbers and chemical reaction rates. *Theor Chem Acc*. **118**(4), 813–26 (2007).
29. Hu, C., Li, H., Zhang, S. & Li, W. A molecular-level analysis of gas-phase reactions in chemical vapor deposition of carbon from methane using a detailed kinetic model. *J Mater Sci*. **51**(8), 3897–906 (2016).
30. Becker, A. & Hüttinger, K. J. Chemistry and kinetics of chemical vapor deposition of pyrocarbon — III Pyrocarbon deposition from propylene and benzene in the low temperature regime. *Carbon*. **36**, 201–211 (1998).
31. Becker, A. & Hüttinger, K. J. Chemistry and kinetics of chemical vapor deposition of pyrocarbon—II Pyrocarbon deposition from ethylene, acetylene and 1, 3-butadiene in the low temperature regime. *Carbon*. **36**, 177–199 (1998).
32. Benzinger, W., Becker, A. & Hüttinger, K. J. Chemistry and kinetics of chemical vapour deposition of pyrocarbon: I. Fundamentals of kinetics and chemical reaction engineering. *Carbon*. **34**, 957–966 (1996).
33. Antes, J., Hu, Z., Zhang, W. & Hüttinger, K. J. Chemistry and kinetics of chemical vapour deposition of pyrocarbon: VII Confirmation of the influence of the substrate surface area/reactor volume ratio. *Carbon*. **37**(12), 2031–9 (1999).
34. Norinaga, K. & Deutschmann, O. Detailed kinetic modeling of gas-phase reactions in the chemical vapor deposition of carbon from light hydrocarbons. *Ind Eng Chem Res*. **46**(11), 3547–57 (2007).
35. Frenklach, M. & Wang, H. Detailed surface and gas-phase chemical kinetics of diamond deposition. *Physical review B*. **43**(2), 1520–45 (1991).
36. Sabbe, M. *et al.* First principle-based simulation of ethane steam cracking. *Aiche Journal*. **57**(2), 482–496 (2011).
37. Ge, Y., Gordon, M. S., Battaglia, F. & Fox, R. O. Theoretical study of the pyrolysis of methyltrichlorosilane in the gas phase. 3. Reaction rate constant calculations. *The Journal of Physical Chemistry A*. **114**(6), 2384–92 (2010).
38. Ziegler, I., Fournet, R. & Marquaire, P. M. Pyrolysis of propane for CVI of pyrocarbon: Part I. Experimental and modeling study of the formation of toluene and aliphatic species. *J. Anal. Appl. Pyrolysis*. **73**(2), 212–230 (2005).
39. Ziegler, I., Fournet, R. & Marquaire, P. M. Pyrolysis of propane for CVI of pyrocarbon: Part II. Experimental and modeling study of polyaromatic species. *J. Anal. Appl. Pyrolysis*. **73**(2), 231–247 (2005).
40. Ziegler, I., Fournet, R. & Marquaire, P. M. Pyrolysis of propane for CVI of pyrocarbon: Part III: Experimental and modeling study of the formation of pyrocarbon. *J. Anal. Appl. Pyrolysis*. **79**(1), 268–277 (2007).
41. Ma, Y., Xue, W., Wang, Z., Ge, M. & He, S. Acetylene cyclotrimerization catalyzed by TiO₂ and VO₂ in the gas phase: A DFT study. *The Journal of Physical Chemistry A*. **112**(16), 3731–41 (2008).
42. Huang, X., Cheng, D., Chen, F. & Zhan, X. The decomposition of aromatic hydrocarbons during coal pyrolysis in hydrogen plasma: A density functional theory study. *Int J Hydrogen Energ*. **37**(23), 18040–9 (2012).
43. Blanksby, S. J. & Ellison, G. B. Bond dissociation energies of organic molecules. *Accounts Chem Res*. **36**(4), 255–63 (2003).
44. Holmen, A. Direct conversion of methane to fuels and chemicals. *Catal Today*. **142**(1–2), 2–8 (2009).
45. Manion, J. A. *et al.* NIST Chemical Kinetics Database, NIST Standard Reference Database 17, Version 7.0 (Web Version), Release 1.6.8, Data version 2015.09, National Institute of Standards and Technology, Gaithersburg, Maryland, 20899–8320, <http://kinetics.nist.gov/>.
46. Cobos, C. J. & Troe, J. The dissociation-recombination system CH₄ + M ⇌ CH₃ + H + M: Reevaluated experiments from 300 to 3000 K. *Zeitschrift für Physikalische Chemie*. **167**(2), 129–149 (1990).
47. Klippenstein, S. J., Georgievskii, Y. & Harding, L. B. Predictive theory for the combination kinetics of two alkyl radicals. *Physical Chemistry Chemical Physics*. **8**(10), 1133 (2006).
48. Stewart, P. H., Larson, C. W. & Golden, D. M. Pressure and temperature dependence of reactions proceeding via a bound complex. 2. Application to 2CH₃ → C₂H₆ + H. *Combustion & Flame*. **75**(1), 25–31 (1989).

49. Tsang, W. & Hampson, R. F. Chemical kinetic data base for combustion chemistry. Part I. Methane and related compounds. *Journal of Physical and Chemical Reference Data*. **15**(3), 1087 (1986).
50. Dean, A. M. Predictions of pressure and temperature effects upon radical addition and recombination reactions. *Journal of Physical Chemistry*. **89**(21), 4600–4608 (1985).
51. Baulch, D. L. *et al.* Evaluated kinetic data for combustion modelling. *J. Phys. Chem. Ref. Data*. **21**, 411–734 (1992).
52. Laufer, A. H. & Fahr, A. Reactions and kinetics of unsaturated C2 Hydrocarbon Radicals. *Chemical Reviews*. **104**(6), 2813–2832 (2004).
53. Hidaka, Y. *et al.* Thermal isomerization and decomposition of 2-butyne in shock waves. *The Journal of Physical Chemistry*. **97**(42), 10977–10983 (1993).
54. Benson, S. W. The mechanism of the reversible reaction: $2C_2H_2 \rightleftharpoons$ vinyl acetylene and the pyrolysis of butadiene. *International Journal of Chemical Kinetics*. **21**(4), 233–243 (1989).
55. Westmoreland, P. R. *et al.* Forming benzene in flames by chemically activated isomerization. *The Journal of Physical Chemistry B*. **93**(25), 8171–8180 (1989).
56. Harding, L. B., Georgievskii, Y. & Klippenstein, S. J. Predictive theory for hydrogen atom? Hydrocarbon radical association kinetics. *The Journal of Physical Chemistry A*. **109**(21), 4646–4656 (2005).

Acknowledgements

The authors gratefully acknowledge the financial support of this study by National Natural Science Foundation of China under Grant No. 51432008, National Natural Science Foundation of China under Grant No. 51872234.

Author contributions

Li, K. and Li, H. designed the calculation models; Li, K. performed the modeling; Li, K., Li, W. and Song, Q. contributed to the data analysis; Li, K. wrote the paper with the support from Yan, N. and Wang, T. All authors contributed to the general discussion.

Competing interests

The authors declare no competing interests.

Additional information

Correspondence and requests for materials should be addressed to H.L.

Reprints and permissions information is available at www.nature.com/reprints.

Publisher's note Springer Nature remains neutral with regard to jurisdictional claims in published maps and institutional affiliations.



Open Access This article is licensed under a Creative Commons Attribution 4.0 International License, which permits use, sharing, adaptation, distribution and reproduction in any medium or format, as long as you give appropriate credit to the original author(s) and the source, provide a link to the Creative Commons license, and indicate if changes were made. The images or other third party material in this article are included in the article's Creative Commons license, unless indicated otherwise in a credit line to the material. If material is not included in the article's Creative Commons license and your intended use is not permitted by statutory regulation or exceeds the permitted use, you will need to obtain permission directly from the copyright holder. To view a copy of this license, visit <http://creativecommons.org/licenses/by/4.0/>.

© The Author(s) 2019